WILEY

CYTOSKELETON

RESEARCH ARTICLE OPEN ACCESS

SEC-SAXS/MC Ensemble Structural Studies of the Microtubule Binding Protein Cdt1 Show Monomeric, Folded-Over Conformations

Kyle P. Smith[1] | Srinivas Chakravarthy[2] | Amit Rahi[1] | Manas Chakraborty[1] | Kristen M. Vosberg[1] | Marco Tonelli[3] | Maximilian G. Plach[4] | Arabela A. Grigorescu[5] | Joseph E. Curtis[6] | Dileep Varma[1]

[1]Department of Cell & Developmental Biology, Northwestern University Feinberg School of Medicine, Chicago, Illinois, USA | [2]Biophysics Collaborative Access Team, Argonne National Laboratory, Argonne, Illinois, USA | [3]National Magnetic Resonance Facility at Madison, Department of Biochemistry, University of Wisconsin, Madison, Wisconsin, USA | [4]2bind GmbH, Regensburg, Germany | [5]Keck Biophysics Facility, Department of Molecular Biosciences, Northwestern University, Evanston, Illinois, USA | [6]NIST Center for Neutron Research, National Institute of Standards and Technology, Gaithersburg, Maryland, USA

Correspondence: Kyle P. Smith (kyle.smith.phd@gmail.com) | Dileep Varma (dileep.varma@northwestern.edu)

Received: 15 August 2024 | **Revised:** 18 October 2024 | **Accepted:** 24 October 2024

Funding: Helium recovery equipment, computers, and infrastructure for data archive were funded by the University of Wisconsin-Madison, NIH P41GM136463, R24GM141526, and by the United States National Science Foundation Mid-Scale Research Infrastructure-1 program under Grant No. 1946970. The use of Pilatus 3 1M detector was provided by grant 1S10OD018090-01 from NIGMS. This work was supported by NIGMS grant R01GM135391 to Dileep Varma.

Keywords: conformational dynamics | intrinsically disordered protein | kinetochore | Monte Carlo | rigid body modeling | small angle x-ray scattering

ABSTRACT

Cdt1 is a mixed folded protein critical for DNA replication licensing and it also has a "moonlighting" role at the kinetochore via direct binding to microtubules and the Ndc80 complex. However, it is unknown how the structure and conformations of Cdt1 could allow it to participate in these multiple, unique sets of protein complexes. While robust methods exist to study entirely folded or unfolded proteins, structure–function studies of combined, mixed folded/disordered proteins remain challenging. In this work, we employ orthogonal biophysical and computational techniques to provide structural characterization of mitosis-competent human Cdt1. Thermal stability analyses shows that both folded winged helix domains1 are unstable. CD and NMR show that the N-terminal and linker regions are intrinsically disordered. DLS shows that Cdt1 is monomeric and polydisperse, while SEC-MALS confirms that it is monomeric at high concentrations, but without any apparent inter-molecular self-association. SEC-SAXS enabled computational modeling of the protein structures. Using the program SASSIE, we performed rigid body Monte Carlo simulations to generate a conformational ensemble of structures. We observe that neither fully extended nor extremely compact Cdt1 conformations are consistent with SAXS. The best-fit models have the N-terminal and linker disordered regions extended into the solution and the two folded domains close to each other in apparent "folded over" conformations. We hypothesize the best-fit Cdt1 conformations could be consistent with a function as a scaffold protein that may be sterically blocked without binding partners. Our study also provides a template for combining experimental and computational techniques to study mixed-folded proteins.

1 | Introduction

Human Cdc10-dependent transcript 1 protein (Cdt1) is a 546-amino acid protein with two well-folded winged helix (WH) domains and two uncharacterized regions. These well-folded domains are referred to as the "middle" WH domain (WHM) and the C-terminal WH domain (WHC) (Figure 1A). Cdt1 was first discovered for its role in origin licensing during DNA replication, where it has been demonstrated to be critical for loading the minichromosome maintenance (MCM) helicase onto the DNA. Even though the WH fold has been established to bind DNA in other contexts, intriguingly, the WHM and WHC domains of Cdt1 have not been demonstrated to bind DNA directly (Pozo and Cook 2016; Xouri et al. 2007). Interestingly, recent studies have shown that Cdt1 also performs an essential, "moonlighting" function during mitosis. It localizes to the kinetochores of condensed chromosomes and the microtubules of the mitotic spindle. This is thought to facilitate specific interactions between these two large mitotic complexes. Cdt1 seems to have gained new aspects of mitotic functionality, as it links the kinetochore-bound nuclear division cycle 80 (Ndc80) complex to polymeric microtubules as well (Pozo and Cook 2016; Xouri et al. 2007).

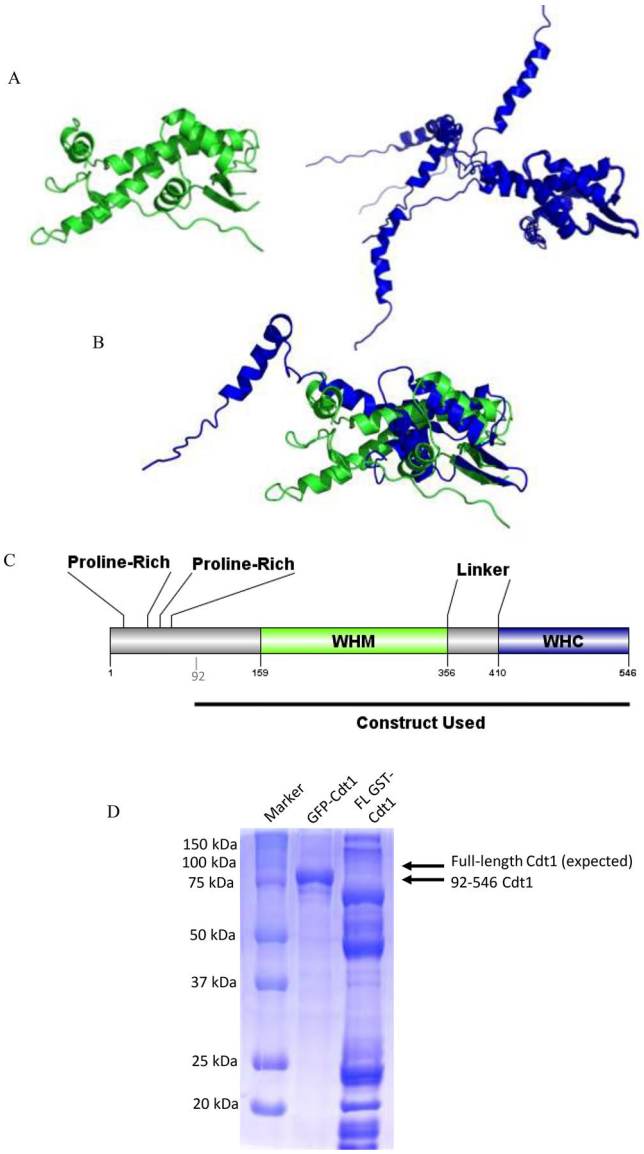

FIGURE 1 | Domain map and published Cdt1 structures. (A) Crystal and NMR structures of the WHM (PDB: 2WVR, green [Lee et al. 2004]) and WHC (PDB: 2KLO, blue [Khayrutdinov et al. 2009]) are shown as cartoons. (B) Overlay of WHM and WHC domains. (C) Full length protein and constructs employed in this and other published studies. (D) SDS-PAGE of one production of Cdt1. Lanes are (1) MW ladder, (2) GFP 92–546 Cdt1 (GFP-Cdt1), and (3) GST-tagged Full-length Cdt1 (FL GST-Cdt1).

Cdt1 has also been enigmatic in that it does not possess any enzymatic activity (Agarwal et al. 2018; Rahi et al. 2023). It has also been shown that the well-folded WHDs of Cdt1 are crucial for their ability to bind microtubules, similar to that of another microtubule-binding protein complex, spindle and kinetochore associated protein 1 (Ska1 [Agarwal et al. 2018; Rahi et al. 2023]). The Ska1 complex, like Cdt1, also associates with Ndc80 at kinetochores. Cdt1 facilitates binding between Ndc80 and Ska1 to form the Ndc80-Cdt1-Ska1 "super complex" that is capable to track plus-ends of spindle microtubules for longer distances and duration than the individual components (Rahi et al. 2023). While Cdt1-contaning complexes required for DNA replication licensing have been well studied, it is unclear how the structure of Cdt1 can mediate specific, defined interactions with other proteins during mitosis. This, combined with our observation that both the WHD's are important for binding to microtubules and Ska1, underscore the importance of investigating Cdt1's structural properties in isolation, which is currently understudied. Further, the alteration of Cdt1 has been critically linked to genomic instability and developmental abnormalities such as primordial dwarfism syndrome (Petropoulou et al. 2008; Pozo and Cook 2016). Given this, structure–function studies of Cdt1 could eventually lead to a better understanding of the pathology of these disease states.

In terms of structural biology, the crystal structure of the mouse WHM domain was first determined in complex with its re-licensing inhibitor, geminin (Lee et al. 2004). Later, the WHM/geminin complex was also determined under higher-order, hetero-oligomeric states (De Marco et al. 2009; Lee et al. 2004). Based on crystallography and small angle x-ray scattering (SAXS) data, in the context of DNA replication, the authors propose that the different inhibitory complexes could allow for what the authors call "licensing-competent" and "licensing-defective states" for the WHM domain. Following the original WHM crystal structure, both the crystal and NMR structures of mouse Cdt1 WHC domain have also been published (Jee et al. 2010; Khayrutdinov et al. 2009), but only as individual, well-folded domains (Figure 1A) with somewhat similar, but still distinct, folds (overlaid in Figure 1B). More recently, advances in single-particle cryogenic electron microscopy (CryoEM) have allowed for a better understanding of Cdt1s function in coordination with the MCM complex during replication licensing (Sun et al. 2013; Yuan et al. 2017, 2020; Zhai et al. 2017). However, notably missing from the previous structural characterization of Cdt1 have been reductionist approaches using the recombinant, multi-domain protein solely in isolation. The currently published data does not provide enough resolution for the structure of Cdt1 alone, an understanding of which is critical to elucidate how Cdt1 enters complex formation with different multimeric protein assemblies during both DNA replication and mitosis. Notably, solution studies, as opposed to cryogenic ones, have been more limited.

As opposed to most folded proteins comprised of α-helices and β-sheets, many other proteins exist as so-called intrinsically disordered proteins (IDP), which are generally flexible in solution. But while IDPs are not completely well-folded, they do not necessarily have completely random coil structure or are entirely unfolded either and can have different local and global structures (Chan-Yao-Chong, Durand, and Ha-Duong 2019; Stelzl et al. 2022). Approximately 50% of proteins in the human proteome are estimated to include at least partial regions of intrinsic disorder (Deiana et al. 2019; Dubreuil, Matalon, and Levy 2019). Therefore, this estimate includes proteins which contain both folded and unfolded portions, most commonly called "mixed-folded" proteins. For Cdt1, unsurprisingly, an amino acid sequence alignment generated by PRALINE shows the linker region that connect the two WH domains is less conserved than the well-folded WH domains themselves (Figure S1A [Simossis and Heringa 2005]), though its structural properties are unknown. Significant work has supported the idea that disordered domains and linkers within proteins can bind to multiple partners with different structures, especially in the case of protein domains connected to each other (Fuxreiter 2020). This can enable mixed-folded proteins to function as scaffold proteins for signaling cascades and as protein–protein interaction "hubs" (Dunker et al. 2005; Wright and Dyson 2015). Historically, disordered proteins were thought to be "undruggable," but there have been more recent cases in which small molecules can bind to and alter the function of disordered protein regions (Neira et al. 2017; Santofimia-Castano et al. 2019). And as a class, these often difficult-to-study mixed-folded proteins have been implicated in schizophrenia (DISC1 [Soares et al. 2011]), polyglutamine disorders (Ataxin [de Chiara et al. 2005]), and microcephaly (Knl1 [Omer Javed et al. 2018]), where treatment options are extremely limited.

Because mixed-folded proteins by definition have both well-folded and disordered regions, unlike structures generated from x-ray crystallography, 3D NMR spectroscopy, and CryoEM, the structure of these proteins often cannot be captured solely by using these higher-resolution techniques. SAXS, however, is an in-solution scattering technique which has been applied to help characterize higher-order protein–protein complexes, protein folding, and IDPs (Kikhney and Svergun 2015). Building upon this, molecular simulation via Molecular Dynamics (MD) and Monte Carlo (MC) approaches to model mixed-folded proteins have provided additional insight into the conformations of mixed-folded proteins. For example, in the case of HIV gag protein, SAXS/MD/MC approaches demonstrated the protein exists in a more compact conformation in solution, in contrast to an extended conformation required for simultaneous membrane and nucleic acid binding during virus assembly (Datta et al. 2007, 2011). Similarly, in the MCM complex, MD/MC approaches allowed for structure/function studies of the disordered regions and relative conformations of the folded domains (Krueger et al. 2014, 2011).

In this study, we employ integrated biophysical, structural, and computational approaches to describe the solution structural ensemble of the intrinsically mixed-folded protein Cdt1. Our modeled conformations suggest that human Cdt1 is folded onto itself, with the WHM and WHC domains close to each other without any apparent inter-molecular self-interaction. Center-of-mass analysis validates these conformations. Our application of orthogonal, complementary biophysical, structural, and computational techniques also provides a template to study other mixed-folded protein systems.

2 | Experimental Procedures

Certain commercial equipment, instruments, materials, suppliers, or software are identified in this paper to foster understanding. Such identification does not imply recommendation or endorsement by the National Institute of Standards and Technology, nor does it imply that the materials or equipment identified are necessarily the best available for the purpose. Unless otherwise indicated, all experiments were performed at the Northwestern University Department of Cell & Developmental Biology (Chicago, IL).

2.1 | Cloning and Molecular Biology

All His_6-GFP-human Cdt1 constructs and vectors were generated as previously described (Agarwal et al. 2018). The constructs were transformed into BL21-CodonPlus (DE3)-RP competent cells (Agilent) for protein expression. Cells were grown in LB media for transformation and precultures. For unlabeled protein expression, proteins were grown in TPM media (20 g tryptone, 15 g yeast extract, 8 g sodium chloride, 2 g dibasic sodium phosphate, 1 g monobasic potassium phosphate into 1 L).

2.2 | Protein Expression and Purification

Conditions were optimized based on the initial protocols from Agarwal et al. (2018). Several changes were made to increase yields. For protein expression, expression and purity were reduced without a fresh BL21 transformation. The induction time was lowered to 3.5 h to minimize proteolysis. After elution from Co^{2+} beads, the protein was concentrated to approximately 500 μL using centrifugal spin filters (Milipore) and injected over a Superdex 200 (S200) Increase 10/300 column (GE Healthcare) connected to an AKTA Pure FPLC (GE Healthcare). Under a flow rate of 0.5 mL/min, His_6-GFP-Cdt1 92–546 eluted at approximately 11.5 mL. The primary contaminant was cleaved GFP. The fractions eluting at approximately 10.5–13.5 mL were pooled, flash-frozen in liquid nitrogen, and stored at −80°C until use. ^{15}N-labeled Cdt1 was purified identically to that of unlabeled protein. Protein was approximately 95% pure by SDS-PAGE (Figure S1B). We assume the higher molecular weight (MW) species are incompletely denatured, and/or contaminant proteins present in the TEV protease itself, and it has been estimated the SDS-PAGE MW markers are ±10% of the actual mass (Wiesner et al. 2021).

2.3 | Commercially Available Proteins

B. taurus carbonic anhydrase isozyme II from erythrocytes, *G. gallus* egg albumin (ovalbumin), *B. taurus* serine albumin,

S. cerevisiae alcohol dehydrogenase, *O. cuniculus* muscle aldolase, *I. batatas* beta-amylase, and *L. mesenteroides* blue dextran were purchased as lyophilized powders or preformulated solutions from Sigma-Aldrich and used without further purification.

2.4 | Protein Tag Cleavage and Buffer Equilibration

For His_6-GFP tag cleavage, 800–1400 μL of approximately 5 mg/mL of protein was incubated with 100 μL of 2 mg/mL TEV protease, provided by the Northwestern Recombinant Protein Production Core. Each reaction was performed in a 1.5 mL tube. The tubes were gently rotated for 1 h at room temperature (approximately 22°C). Samples were put on ice, concentrated to approximately 300 μL and injected over a S200 Increase 10/300 column. Using a flow rate of 0.5 mL/min, cleaved Cdt1 92–546 eluted at approximately 12.2 mL and 11.5–12.5 mL were pooled, concentrated, and flash frozen in liquid nitrogen. To buffer exchange the proteins into the appropriate assay buffer before assay use, SEC using an S200 was employed to both buffer exchange and ensure folded, active samples distinct from potential aggregates. The protein concentration of tag-cleaved Cdt1 92–546 was calculated using the theoretical extinction coefficient (Gasteiger et al. 2005) of all tryptophan, tyrosine, and reduced cysteine residues in our construct at 280 nm (21,930 $M^{-1}\,cm^{-1}$) on a NanoDrop 1000 spectrophotometer (Thermo Fisher).

2.5 | Cdt1 Expression for Isotopic Labeling

For ^{15}N labeling of Cdt1, 1 L cultures of autoinduction media (Cold Spring Harbor Protocols) were used with ^{15}N labeled ammonium chloride (Cambridge Isotope Laboratories). The final antibiotic concentration was increased to 0.1 mg/mL of kanamycin to reduce plasmid loss and poor yields. Cultures were grown in 2.5 L Ultra Yield flasks (Thomson Instrument Company) for increased aeration. 1 L cultures were inoculated with 5.0 mL of overnight preculture cells. The cultures were grown in darkness at 37°C with shaking at 250 rpm until an OD_{600} of 0.6, when the temperature was lowered to 30°C overnight. The cells continued to grow for approximately 16 additional hours. Cell pelleting, lysis and purification were identical to that of the unlabeled protein.

2.6 | TIRF Microscopy

A microscopy perfusion chamber was prepared by attaching an acid-washed coverslip (22 × 22 mm, thickness 1½, Corning) over a precleaned glass slide (75 × 25 mm, thickness 1 mm, Corning) using a double-sided tape (Scotch) resulting in a chamber volume of approximately 10 μL. For more details, see the previously published TIRF-M Materials and Methods section (Afreen et al. 2022). Acid-washed coverslips were further cleaned by holding them under flame for a couple seconds before use. Solutions were then exchanged into the perfusion chamber with a micropipette and filter paper. The chamber was activated by flowing in the following solution in the order in which they appear below, followed by incubation for 5 min and intermittent washing with three chamber volumes of buffer B (MRB80, [80 mM potassium PIPES, 1 mM EGTA, 4 mM $MgCl_2$, pH 6.8], supplemented with 10 μM taxol), PLL PEG biotin (0.1 mg/mL, Susos, AG), streptavidin (0.625 mg/mL, S4762, Sigma), diluted solution of taxol stabilized microtubules (1 in 100 dilutions form the stock), and κ-casein (1 mg/mL). All incubations were done inside a wet chamber to prevent evaporation. A solution of cleaved Cdt1 (100 nM, in buffer B) was subsequently flown into the chamber and incubated for 5 min. The chamber was then washed with the following antibody solutions: anti-Cdt1 (1 in 500 dilution in buffer B), and Alexa488 labeled-secondary antibody (1 in 1000 dilution in buffer B) with intermittent washing with buffer B. The chamber was finally washed with imaging buffer (MRB80 supplemented with 10 μM taxol, 0.6 mg/mL^{-1} κ-casein, 4 mM DTT, 50 mM glucose [#G8270, Sigma], 0.2 mg/mL, catalase [#C9322, Sigma], and 0.4 mg/mL glucose oxidase [#G7141, Sigma]). Images were recorded using the following microscopy settings. Images were recorded using a Nikon Ti-2 inverted microscope equipped with an Andor iXon3 CCD camera (Cambridge Scientific, Watertown, MA, USA), 1.49× NA, and 100× oil objective. The microscope produced 512 × 512-pixel images with 0.16 μm per pixel resolution in both *x* and *y* directions. NIS-elements software (Nikon) was used for data acquisition with 100 ms exposure times. Microtubule images were collected using a 640 nm excitation laser and Alexa 488 labeled antibody images were collected using a 488 nm laser excitation line.

2.7 | SEC-MALS

Experiments were performed at the Northwestern University Keck Biophysics Facility (Evanston, IL). Solution size exclusion chromatography coupled with multi-angle laser light scattering/quasi-elastic light scattering (SEC-MALS/QELS) experiments were conducted using Agilent Technologies 1200 LC HPLS system (Agilent Technologies, Santa Clara, CA) equipped with a Wyatt Dawn HeleosII 18-angle MALS light scattering detectors, Optilab T-rEX refractive index detector, WyattQELS quasi-elastic (dynamic) light scattering (QELS) detector and ASTRA software (Wyatt Technology Europe GmbH). QELS interval was set to 0.5 s and the collection interval was set to 0.4 s. Cdt1 92–546 was at a concentration of 3.53 mg/mL and was cleaved/purified the prior day before overnight storage at 4°C. A total of 250 μL of each protein was injected and run on a S200 Increase 10/300 column (GE Healthcare) at a flow rate of 0.40 mL/min in SEC-MALS buffer (10 mM Tris pH 8.3, 150 mM NaCl, 0.25 mM TCEP) at room temperature (24.3°C). Monomeric bovine serum albumin was used to experimentally determine the dn/dc value (0.161 mL/g) under our conditions. The refractive index was set to 1.335 and the viscosity was set to $8.9450 \times 10^{-3}\,g\,cm^{-1}\,sec^{-1}$. R(h) analysis was based on Saad Tayyab and Islam (1991). The elution volume reported is the normalized A280 value. Void volume (Vo) was measured using a 250 μL injection of 7.89 mg/mL blue dextran (Sigma-Aldrich). Inclusion volume (Vi) was measured using a 250 μL injection of 2% ethanol (v/v). R(h) values were reported as previously published. Each protein standard was resuspended in SEC-MALS buffer to 2.0–8.0 mg/mL and syringe filtered through a 0.22 μm filter before injection of 250 μL.

2.8 | Intrinsic Fluorescence DSF (nanoDSF)

Experiments were performed at 2bind GmbH (Regensburg, Germany). Cdt1 and ovalbumin were diluted from stock concentration (6.35 and 10 mg/mL, respectively) to 5 μM in "Stability Buffer" (25 mM HEPES pH 7.4, 150 mM NaCl). Duplicate samples were loaded into standard nanoDSF glass capillaries and analyzed on a Prometheus NT.48 device with additional back-reflection optics (NanoTemper Technologies, Munich, Germany). The fluorescence at 350 and 330 nm was measured while the temperature was increased from 20°C to 95°C at a rate of 1.0°C/min. Excitation power was set to 70%. Thermally-induced aggregation (T_{agg}) was also inferred by measuring light-scattering while increasing the temperature from 20°C to 95°C at a rate of 1.0°C/min. Based on the number of capillaries, data were recorded approximately every 0.02 s. Data were analyzed using PR. ThermControl (v2.0.4) software (NanoTemper Technologies, Munich, Germany). Thermal melting temperatures (T_m) were inferred from inflection points of 350/330 nm fluorescence ratio curves in first approximation.

2.9 | CD Spectroscopy

Experiments were performed at the Northwestern University Keck Biophysics Facility (Evanston, IL). Data were collected on a Jasco J-815 CD Spectrophotometer (Jasco Analytical Instruments, Easton, MD). A flow rate of 1.70 m^3/min nitrogen was used to purge the system of oxygen and was kept running throughout the experiments. Proteins were kept on ice before CD experiments to ensure they remained properly folded. For secondary structure assignment, approximately 75 μL of 1.16 mg/mL (54 μM) protein in CD buffer (10 mM Tris pH 8.3, 150 mM NaCl, 0.5 mM TCEP) was put into a 0.1 mm slide cuvette (Hellma Analytics). Data integration time was set to 4 s; bandwidth was set to 2.0 nm, and three accumulations were in "step" scanning mode. HT was also monitored and remained less than 600 V at all wavelengths. CD spectra were recorded from 180 to 260 nm using a step size of 1 nm. Six initial preliminary spectra were collected for differential scanning measurements to optimize path length, protein concentration, and buffer concentration. Final data collection was performed with 300 μL of 0.193 mg/mL (9 μM) protein in diluted CD buffer (6 mM Tris pH 8.3, 90 mM NaCl, 0.3 mM TCEP) in a 1 mm cuvette (Hellma Analytics). The sample was heated from 10°C to 90°C with a 1.0°C/min temperature increase. The data were collected every 1.0°C at 209 and 220 nm wavelengths, corresponding to local minima observed for the spectrum collected at 25°C. Temperature was held constant during data collection measurements. Data integration time was set to 1 s; bandwidth was set to 2.0 nm, and one accumulation was in "continuous" scanning mode. HT was also monitored and remained less than 600 V at all wavelengths. CD spectra were recorded from 195 to 280 nm. Data analysis was performed in the Spectra Manager Ver.2 software package using the CD pro analysis and protein denaturation analysis portions. CONTIN (Provencher and Glockner 1981) was used to assign the secondary structure. Three CONTIN soluble protein databases (SP29 [178–260 nm], SP37 [185–240 nm], and SP43 [190–240 nm]) were used to fit the CD spectrum. The percentages of secondary structures were averaged from the fittings of each database. The root mean square deviation (RMSD) and normalized root mean square deviation (NMRSD) show the goodness of fit and were around 3% and 2%, respectively. The melting temperatures extracted from the fit are within less than 0.5°C difference (209 nm: 42.0°C ± 0.2°C and 220 nm: 42.4°C ± 0.2°C).

2.10 | DLS

DLS measurements were performed using a Punk 0037 Dynamic Light Scattering Analyzer (Unchained Labs). Each sample was loaded into a disposable 5 μL sample holder (BladeCell) and measured at 20°C. Intensity-weighted size distribution was obtained over 10 runs of five measurements each. The solvent was recorded as PBS and its refractive index of 1.3 mol/L was assumed. The optical attenuator and laser intensity parameters were set automatically for each run. The determined R(h) was interpolated from the average of three technical replicates using one protein production. One replicate was discarded because it had a poorer fit to the correlation function. One other replicate was discarded because it was 1.5× the standard deviation of the average of the other three replicates.

2.11 | NMR Spectroscopy

Experiments were performed at NMRFAM at the University of Wisconsin (Madison, Wisconsin). ^{15}N labeled Cdt1 92–546 was concentrated to 200 μM in 10 mM HEPES, 150 mM NaCl pH 7.4 buffer before dilution in 10% D_2O (v/v, Sigma) and placed in a 5 mm NMR microtube susceptibility matched to the solvent (Shigemi). Data were collected at 15°C on a Bruker Avance III HD spectrometer operating at 900 MHz (^1H) and equipped with a cryoprobe. Two-dimensional ^1H–^{15}N-TROSY-HSQC spectra were recorded with 1024 and 100 complex points in the ^1H and ^{15}N dimensions, respectively. Each FID was accumulated with 192 repetitions and 1.5 s recovery delay (D1). The ^1H direct dimension was centered on the signal from water at 4.87 ppm with a spectral width of 16.3 ppm, while the ^{15}N indirect dimension was centered at 118.7 ppm with a spectral width optimized to 31.3 ppm. All the spectra were processed using NMRPipe (Delaglio et al. 1995) and analyzed in the NMRFAM-SPARKY (Lee, Tonelli, and Markley 2015) software package.

2.12 | SEC-SAXS

Experiments were performed at the Advanced Photon Source BioCAT beamline (Sector 18-ID) of Argonne National Laboratory (Argonne, IL), as described by Mathew, Mirza, and Menhart (2004). The 12 keV x-ray beam (λ = 1.033 Å) was focused on a 1.5 mm quartz capillary sample cell with 10 μm walls. The scattering, in the momentum transfer range, $q = 0.0038–0.4$ $Å^{-1}$, was collected on a Dectris Pilatus3 × 1M detector approximately 1.5 m downstream of the sample

position. All instrumentation and experiments were performed at 25°C. About 275 μL of 5.64 mg/mL Cdt1 92–546 in storage buffer (25 mM Tris pH 8.3, 500 mM NaCl, 0.5 mM TCEP, 5% sucrose [w/v]) was fed into the x-ray beam after passing through a S200 Increase 10/300 GL column (GE Healthcare) in SAXS buffer (50 mM HEPES pH 7.4, 500 mM NaCl, 1 mM TCEP). A flow rate of 0.75 mL/min was used. The delay between the protein emerging from the SEC column and its arrival at the beam position was approximately 1 min. SAXS exposures with a length of 0.5 s were collected every 3.0 s. Scattering data were radially averaged, processed, scaled, and analyzed using PrimusQT (Konarev et al. 2003). Exposures before and after sample elution were averaged and used as buffer background. Frame 319 of 530, in the center of the eluted SEC peak, was used for further analysis. Pair distribution functions, P(r), of the scattering centers were computed from the scattering curves using GNOM (Franke et al. 2017). Guinier analysis was performed using RAW (Hopkins, Gillilan, and Skou 2017).

2.13 | Molecular Simulations

The starting model was generated using the x-ray structure of human Cdt1 WHM (PDB: 2VWR, 8) and a human homology model of mouse Cdt1 NMR structure (PDB: 2KLO, 10). Residues 90–166 and 354–410 were added as initially linear sequences using PSFGEN and NAMD (Phillips et al. 2005). The model was prepared using the CHARMM-32 force field (Best et al. 2012). The initial structure was energy minimized and relaxed via 1 ns NVT MD simulation. Subsequent MC simulations were completed using the Monomer MC module in the program SASSIE (41), with residues 90–163 and 351–443 denoted as "flexible." Simulations were performed at 300 K. After 500 attempts with a steric clash, the simulations were returned to the previous structure. Around 13,724 out of an attempted 250,000 non-overlapping accepted structures were each energy minimized and used for subsequent analysis using SASSIE modules Chi-Square Filter and Density Plot. Structures were generated using MC analysis, as previously published (Curtis, Hirsh, and Susan 2012). Analysis of domain distributions from the ensemble was done by calculating the center-of-mass for all atoms in the WHM (residues 160–350) and WHC (residues 410–546) domains for each structure in the trajectory.

2.14 | Graphics

Sequence alignment was visualized using PRALINE (Simossis and Heringa 2005). Domain maps were drawn using DOG (Ren et al. 2009). Protein ribbon diagrams were visualized using PyMOL ("The PyMOL Molecular Graphics System, Version 2.0 Schrödinger LLC." [Schrödinger LLC 2020]). TIRF-M images were generated in Nikon image software and exported as TIFF files. Thermal stability, spectroscopy, DLS, SEC-MALS, and SEC-SAXS figures were visualized using Excel (Microsoft). HSQC spectra were visualized using NRMFAM (W. Lee, Tonelli, and Markley 2015). Density plots were generated using SASSIE and visualized using VMD (Humphrey, Dalke, and Schulten 1996).

3 | Results and Discussion

3.1 | Human Cdt1 92–546 Is Competent in Binding to Microtubules

We previously predicted the N-terminal 1–92 region of Cdt1 to be disordered partially based on its 18.5% proline content (Agarwal et al. 2018), which is approximately three times higher than across the human proteome (Morgan and Rubenstein 2013). Based on our previous studies, we predicted that these N-terminal motifs would likely be proteolyzed during expression if they remained a part of the construct (Agarwal et al. 2018; Rahi et al. 2023). And to our knowledge, no group has been able to produce full-length, recombinant Cdt1 protein in the absence of its replication licensing binding partners. When we attempted to express and purify a GST-tagged version of full-length Cdt1, we observed, as expected, this protein was highly susceptible to proteolysis, visualized as lower MW bands in SDS-PAGE. The largest intact fragment (amino acids 92–546) was predominantly stable in solution (Figure 1C,D). Further, we have demonstrated this largest fragment of human Cdt1 is completely able to carry out its mitotic functions at kinetochores and spindle microtubules in HeLa cells (Agarwal et al. 2018; Rahi et al. 2020). These functions depend on Cdt1's ability to bind to the microtubules, the Ndc80 complex and the Ska1 complex during mitosis. Since the primary focus of our work is on the mitotic function of Cdt1, all our experiments were conducted with the largest fragment of human Cdt1, hereafter referred to just as "Cdt1" (Figure 1C,D), representative of a mitosis-competent construct in vitro.

As a control and reference protein, we used ovalbumin, which has a MW similar to Cdt1, is very well-folded with alpha helices as well as beta sheets, and is very well-characterized structurally. We had previously demonstrated that a GFP-tagged version of Cdt1 92–546 binds directly to microtubules by using both microtubule co-pelleting and total internal reflection fluorescence microscopy (TIRF-M) binding assays (Agarwal et al. 2018). To ensure that the cleaved Cdt1 92–546 molecule also retained the ability to bind microtubules, we carried out a TIRF-M assay to test this. The methodology resembled an indirect immunostaining experiment (see Section 2) where we used a primary antibody to detect Cdt1 and then a fluorescently labeled secondary antibody to visualize Cdt1 molecules bound to immobilized microtubules. We observed that this tagless Cdt1 protein overlays with microtubules, as opposed to the control protein ovalbumin, confirming that Cdt1 binds to polymerized microtubules in vitro (Figure 2A). This demonstrates that our construct binds directly to microtubules, as expected.

3.2 | Thermal Denaturation Experiments Demonstrate That Cdt1 Is Unstable

To study the thermal stability of Cdt1, we performed differential scanning denaturation experiments. We used circular dichroism (CD) and intrinsic protein fluorescence (Ex280, Em330/350) to measure the changes in secondary and tertiary

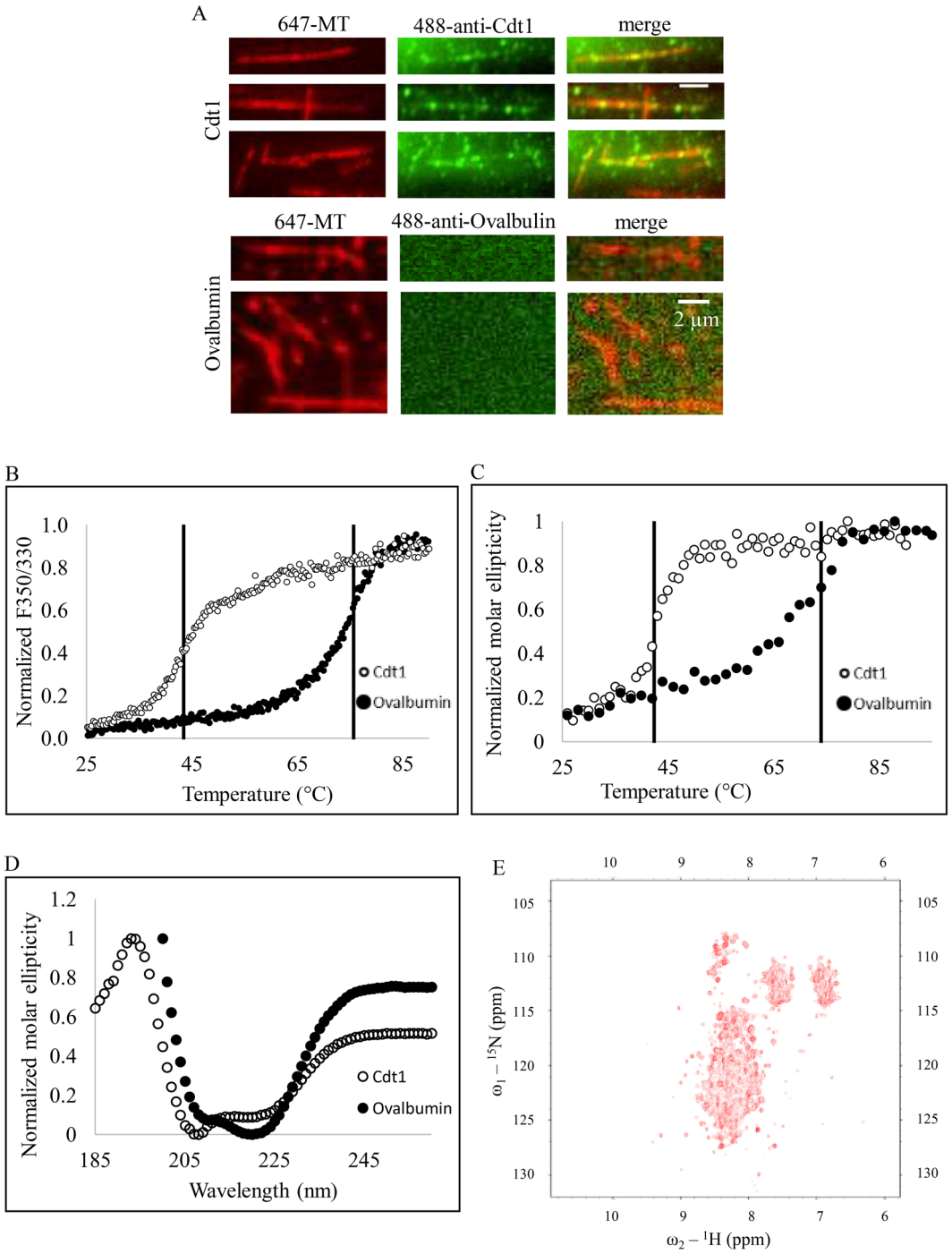

FIGURE 2 | Microtubule binding, thermal denaturation, and spectroscopic analyses of Cdt1. (A) TIRF-M analysis of Cdt1-microtubule binding. Microtubules are shown in red, and ovalbumin/Cdt1 is shown in green. Scale bars represent 2 μm. (B) DSF of Cdt1 and ovalbumin. The normalized F350/330 ratio is plotted as a function of temperature. Vertical lines represent melting temperatures. Ovalbumin is plotted in closed circles and Cdt1 in open circles. (C) DSCD of Cdt1 and ovalbumin. Normalized molar ellipticity is plotted as a function of temperature. (D) CD spectra of Cdt1 and ovalbumin. The normalized CD is plotted as a function of wavelength. (E) ^{15}N–^{1}H TROSY HSQC of Cdt1. ^{15}N and ^{1}H signals are plotted in ppm.

elements, respectively. In both methods, the protein is heated until thermal denaturation and unfolding, with the detection being either circularly polarized light (CD), or intrinsic tryptophan fluorescence (FL). Our thermal stability data for ovalbumin (Figure 2B,C) were similar to previously published data (Ito and Matsudomi 2005) given the difference in buffers (Table S1). For both differential scanning fluorimetry (DSF) and differential scanning circular dichroism (DSCD), Cdt1 appeared to primarily follow a simple two-state unfolding process, where only one transition, or inflection point, is observed during thermal denaturation. Using fluorescence detection, we observed 50% of the protein being unfolded at a melting temperature (T_m) of 43°C (Figure 2B). In CD, we determined a T_m of 42°C (Figure 2C). Both domains unfold simultaneously. The low T_m values relative to physiological 37°C demonstrate that Cdt1 is intrinsically unstable.

3.3 | Spectroscopic Characterization Demonstrates Significant Intrinsic Disorder in the N-Terminus and Linker Regions

To experimentally determine the unstructured content of the protein, we used CD and NMR spectroscopy to assess the secondary structure. In protein CD, the spectral features correspond to specific secondary structure elements, and proteins of the same size will have different spectra depending on secondary structure composition. Our CD secondary structure assignment for the ovalbumin spectra (Table S2) was similar to the published x-ray crystal structure under our conditions (Stein et al. 1991). In Cdt1, the CD spectra indicate that a large portion of the protein is neither helical nor sheet (Figure 2D, Table S3), and approximately 50% of is in the "random coil" region, which peaks around 200 nm (Chemes et al. 2012; Greenfield 2006). In-solution methods, such as CD, can show an increased "unstructured" content compared with x-ray crystal structures and 1D domain maps due to the presence of unstructured loops in between secondary structure elements, and, frequently, less crystal packing and hydration restraints. These inter-secondary structure elements are sometimes referred to as "disordered," though in CD, they would be more closely defined as "unstructured" which includes loops and inter-strand structures.

We then collected an $^{1}H/^{15}N$-TROSY-HSQC NMR spectra to validate our CD results (Figure 2E). Each of the H–N backbone bonds generate a peak in the NMR spectra, whose physical location in the HSQC spectra depends on the secondary structure of said backbone atoms. Analyzing the spectrum with NMRFAM-SPARKY (Lee, Tonelli, and Markley 2015), we note a flexible portion of the protein yields strong peaks with poor peak dispersion and a structured portion of the protein with peaks with good dispersion. Given the relatively large size of the protein, the peaks from the structured part will relax faster (shorter T2) and appear broader and weaker than the peaks from the unstructured regions parts that relax much slower (longer T2). The number of peaks (482 discernable peaks of an expected 535), their broadness, and their location similarly demonstrate a high disorder content (Lee et al. 2012; Yao, Dyson, and Wright 1997). From our NMR data, we estimate approximately 100 strong peaks that correspond to unstructured residues, consistent with our estimates from CD that the N-terminal and linker regions are completely disordered. This contrasts the equally sized, well-folded maltose binding protein (BMRB entry #7114). Studying structural changes via NMR at different temperatures could allow for better understanding of the stability of the secondary structure. This data confirms all but the WH domains are disordered in human Cdt1.

3.4 | Hydrodynamic and Scattering Experiments Show That Cdt1 Is a Monomeric, Mixed-Folded Protein With Significant Conformational Heterogeneity

After validating that Cdt1 contains disordered regions at the N-terminus and WH domains' linker, we used scattering and chromatography techniques to further investigate the biophysical properties. We used dynamic light scattering (DLS) to estimate the hydrodynamic radius (R(h)) and polydispersity of Cdt1 in solution. In DLS, a monochromatic beam of light is scattered by the sample, the rate of intensity fluctuation is measured, and properties like radius and conformational heterogeneity can be inferred from the solution diffusion behavior. Ovalbumin showed similar R(h) values in our system (Figure S2A) compared with published results (Smilgies and Folta-Stogniew 2015). For Cdt1, the single peak in DLS demonstrated the protein was 99% monomeric and has an R(h) of 3.7 nm even though it is 40% polydisperse, as demonstrated by the increased width of the peak (Figure 3A). This relatively high level of polydispersity is consistent with a mixed-folded protein with many different conformations and also consistent with our observed thermal instability at relatively low temperatures (Shiba et al. 2010).

Size exclusion chromatography coupled with multi-angle light scattering (SEC-MALS) can orthogonally determine the hydrodynamic radius, MW, and oligomeric state (Some et al. 2019). SEC separates the sample according to hydrodynamic radius, while the MALS laser light scattering allows for absolute MW determination in solution and thus, the oligomeric state. Our SEC system demonstrated an excellent correlation between our experimental elution volume and previously published R(h) values for six SEC standard/model proteins (Saad Tayyab and Islam 1991; Smilgies and Folta-Stogniew 2015). Analysis of the standards demonstrated our system was accurate to, on average, ±10% in mass from published values (Figure S2B and Table S4). When we tested Cdt1, it eluted significantly earlier than expected for a well-folded protein of similar MW to ovalbumin. However, it eluted significantly after the Vo and the tetrameric beta-amylase, consistent with a mixed folded protein rather than aggregate. Notably, with sensitive UV detection, no apparent higher MW species were observed on the leading edge of the main peak. Assuming no column resin interactions, based on interpolation of model protein SEC elution times (Saad Tayyab and Islam 1991), we interpolated the R(h) of Cdt1 to be 4.4 nm (Table 1 and Figure S2C–F). MALS determined this Cdt1 construct to be 46 kDa, within 10% of the theoretical monomer MW from *in silico* calculations (Figure 3B and Table 1). We noted that the measured MW remained constant throughout the peak at various concentrations, as demonstrated by a relatively flat, consistent MW measurements. Due to this, we infer there may be limited inter-molecular self-association or transient oligomers under our conditions, which would otherwise appear as a sloped measured MW line with different MWs determined across the peak (Some et al. 2019).

To build on the DLS and SEC-MALS experiments, we performed size exclusion chromatography coupled with small-angle x-ray scattering (SEC-SAXS [Smilgies and Folta-Stogniew 2015]) for higher-resolution structural information. SAXS, on its own, uses x-ray scattering to infer structural properties at lower resolution than crystallography. However, it is run in a solution, liquid state rather than the generally artificial environment of a protein crystal. Using SEC upstream of SAXS allows for improved buffer subtraction, removal of particles and aggregates, and separation of oligomers which could otherwise confound SAXS analysis in batch mode (Malaby et al. 2015; Watanabe and Inoko 2009). As the protein is separated via SEC, different SAXS frames across the peak can capture the radius of gyration (Rg) and oligomeric state at various protein concentrations (Graewert et al. 2020). The structural data inferred from our SAXS data

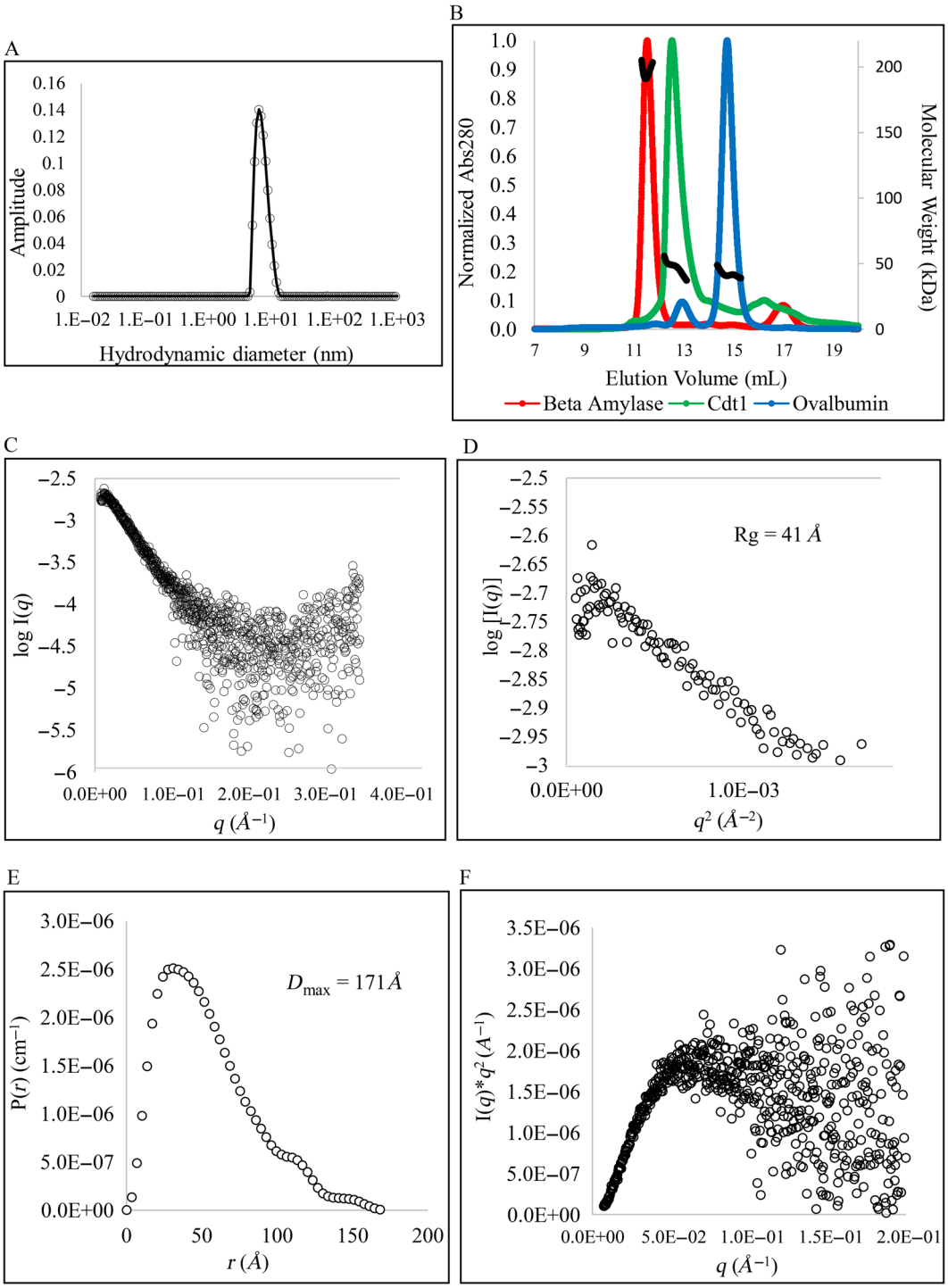

FIGURE 3 | Hydrodynamic and scattering analyses of Cdt1. (A) DLS mass distribution for Cdt1. Amplitude is plotted as a function of the log of hydrodynamic diameter (nm). (B) SEC-MALS chromatogram of Cdt1 and model proteins. Normalized concentration (Abs280) and determined MW (kDa) are shown as a function of elution volume (mL). Red is beta-amylase, green is Cdt1, and blue is ovalbumin. (C) Normalized scattering plot of Cdt1. Log scattering intensity [Log(I)] is plotted as a function of scattering angle (Å^{-1}). (D) Guinier plot of Cdt1. The natural log of intensity (Ln(I) in relative units) is plotted as a function of scattering angle (Å^{-1}). (E) Distance distribution function. The distribution of distances between all pairs of points within the protein (P(r)) is plotted as a function of radius (Å). (F) Kratky plot. I^*q^2 is plotted as a function of scattering angle (q).

for ovalbumin were comparable to previously published values for the well-folded protein (Figure S3A–D [Ianeselli et al. 2010]). Cdt1 scattering data were analyzed further in depth from one frame in the middle of the SEC peak (see Section 2). Only frames corresponding to relatively high protein concentrations yielded a strong enough signal for downstream Guinier and Rg analyses. Additionally, MALS demonstrates monomer throughout the peak with a significantly higher sensitivity and sampling rate than SAXS.

Normalized scattering is shown in Figure 3C. For Cdt1, under our conditions, analysis of the Guinier region from $q^2 = 0.0001$

TABLE 1 | Biophysical properties of Cdt1.

Parameter	Value
Aggregate SEC R(h) (Å)	44
DLS R(h) (Å)	37
SAXS Rg (Å)	41
SAXS D_{max} (Å)	171
MALS MW (kDa)	46
Theoretical MW (kDa)	51

to 0.0011 (Figure S4A,B) shows an Rg of 41 Å. The deviation from linearity at higher scattering angles, that is $q^2 > 0.0025$, compared with ovalbumin in Figure S3B, is expected for a partially disordered protein with a q_{max}*Rg > 1.1 (Borgia et al. 2016; Zheng and Best 2018). The Rg (Figure 3D), calculated from a linear fit of (Figures 3D and S4A,B) and maximum diameter (D_{max}) values, where P(r) = 0 at the *x*-axis (Figure 3E), were also noticeably larger than globular ovalbumin (Tables 1 and S5). For Cdt1, the tailing of the P(r) plot and a Kratky plot which did not return to the *x*-axis after $q > 0.05$ (Figure 3E,F) are both consistent with a partially unfolded protein. These solution scattering results, and the Rg/R(h) ratio, validate that Cdt1 contains both significant folded and unfolded regions. The experimentally determined Rg values were also independent of protein concentration across the SEC elution peak, where the calculated Rg values in dots were all approximately 41 Å (Figure S4C). In agreement with our MALS data (Table 1), our SAXS data are consistent with the interpretation that there were no significant inter-molecular interactions, self-association observed, or higher order oligomerization under the conditions tested, which otherwise would have shown a change in MW or Rg as a function of SEC elution time. We interpret both our SEC-MALS and SEC-SAXS data as Cdt1 being monomeric with minimal inter-molecular self-interactions, even at injection concentrations as high as 110 μM in vitro (see Section 2).

3.5 | Ensemble Rigid Body Modeling Suggests the Two Folded Domains of Cdt1 Are Spatially Close to Each Other in "Closed" Conformations

To better understand the structural conformations of folded and unfolded regions, we combined experimental and computational approaches using SAXS/MD/MC from the web server SASSIE (Curtis, Hirsh, and Susan 2012; Perkins et al. 2016). By combining experimental SAXS data with molecular simulations, "conformational space" can be better sampled and SAXS/MD/MC can access structural information that is otherwise difficult to capture solely by experimental means (Chan-Yao-Chong, Durand, and Ha-Duong 2019). The SASSIE workflow is shown in Figure S5A, and additional simulation details are included in the Section 2. In brief, using our input experimental SEC-SAXS data with SASSIE, we (1) created an initial model using the WH domains as rigid bodies (PDB: 2WVR and 2KLO) with the experimentally determined unstructured regions defined as "flexible" for a "beads-on-a-string" model, (2) generated an ensemble of structures using a "random walk," (3) simulated the theoretical SAXS curve for each ensemble structure, and then (4) analyzed the best-fit conformations using Rg and χ^2 filters. With this approach, we aim to understand possible conformations for mixed-folded systems like Cdt1.

We defined the N-terminal and linker regions as entirely flexible based on our experimental secondary structure content analysis above. While machine learning approaches like AlphaFold (Jumper et al. 2021), RoseTTAFold (Baek et al. 2021), and others have broadly advanced the understanding of protein folds, they are not suitable for use in Cdt1 in this context. Cdt1 is not a continuously folded protein, and we are studying the inter-domain movements rather than a single, static structure generated by AlphaFold. Further, multiple AlphaFold models of Cdt1 that we generated months apart yielded completely different structures (not shown) where the orientation of the two WH domains did not come close to a consensus. Without an AlphaFold consensus of where the WHC domain is placed relative to the WHM domain, our starting model and ensemble approach is as valid as any other for further analysis.

Using "random walk" simulations, we first generated a total of 250,000 structures, of which 13,724 were accepted based on steric hinderance. This "conformational space" is shown as black dots in Figure 4A and black mesh in Figure 4B. We then filtered the data according to models that best-fit both our experimental Rg and χ^2 fit to the scattering curve. Only 3945 had a $\chi^2 < 3$ to the experimental scattering data, shown in blue in Figure 4A,B.

Representative models generated are shown in Figure 4C and Table 2. The best, worst, and average computational fits to experimental data are shown in Figure S5B. Model 1, with a highly compact conformation, had an Rg that was too low to fit our SAXS data. Model 2 structures had accurate Rg values, but did not have a low χ^2 fits to our *q* versus *I*(*q*) plot. Similarly, the Model 3 "extended" conformations, with the two domains spaced approximately 140 Å apart, are among the worst fits to our data.

The best-fit data, represented by Model 4, is shown in Figure 4C and has an χ^2 value of 1.7 and an Rg of 41 Å, remarkably similar to our SEC-SAXS scattering curve and Rg. Conformations like Model 4 are those where the WHM and WHC domains are close, with the N-terminal and linker regions being extended into the solution (Figure 4D). The "best-fit" Model 4 shown is merely a single, representative structure of all configurations in the ensemble which have low χ^2 values. A comparison of the folded Cdt1 domains with the ovalbumin shows that these linker and N-termini regions are likely responsible for the increased R(h) and Rg (Figure S5C). Despite having stretches of 67 and 54 amino acid disordered regions respectively, and no signs of inter-molecular self-interaction via scattering techniques, the two WH domains are only approximately 20 Å apart from each other at their closest in Model 4. We refer to this best-fit conformation as "folded over." Unfortunately, yeast Cdt1 has an additional folded domain (Frigola et al. 2017) and is only 39% similar to human Cdt1, making it difficult for structural comparisons to those at the pre-replication complex (Pozo and Cook 2016).

We also calculated the inter-domain distances of this ensemble from the WH center-of-masses. The WHM and WHC

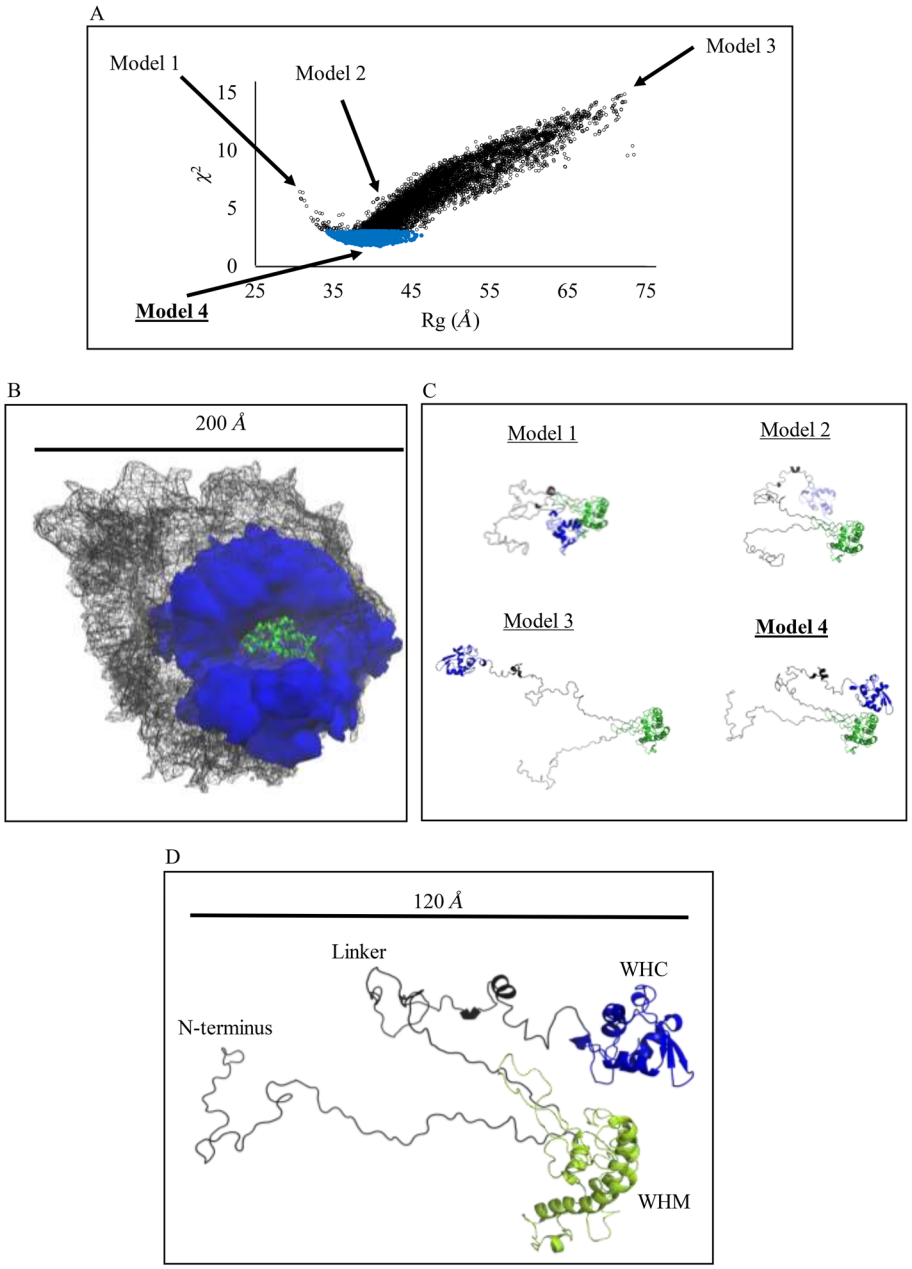

FIGURE 4 | SAXS/SASSIE rigid body modeling of Cdt1. (A) Plot of Rg versus χ^2. All generated models are shown in black where models with a χ^2 value less than three are colored blue. Arrows and labels indicate representative models. (B) Ensemble of structures. The total accepted steric conformational space is shown in black mesh, while experimental well-fit conformations are shown in blue. (C) Representative conformations. The WHM domain is fixed and shown in green. The WHC domain is in blue. N-terminal, and linker regions are in black. Models are elaborated on in the text. (D) Enlargements of a representative best-fit Model 4 from panel C.

boundaries used in Figure 1A, and historically, were used as domains. Because each WH domain probably binds to distinct sites in its protein complexes, studying Cdt1's inter-domain center-of-mass would validate our SASSIE simulations and be useful for future comparisons. Calculations for each of the four models are shown in Table 2. The distribution of inter-domain distances was broad, given the range and number of structures derived from the MC simulations (Figure 5A). Only structures with inter-domain distances between 35 and 52 Å had $\chi^2 < 2$ and fit our data (Figure 5B). As expected, this distribution was slightly larger for those structures with $\chi^2 < 3$ (Figure 5C). And for $\chi^2 > 5$, only poor-fitting structures were abundant (Figure 5D). From this analysis, χ^2 best-fit values and χ^2 worst-fit values agree with our SASSIE-generated ensemble and are consistent with "folded over" conformations as well-fit structures.

4 | Conclusions

To better understand the structure and function of Cdt1, we performed orthogonal biophysical experiments and computational simulations. Our thermal denaturation experiments conclusively determined that Cdt1 is unstable. Some reports anecdotally correlate low protein stability in vitro with low stability in vivo (Foit et al. 2009; Ghaemmaghami and Oas 2001; Ulery-Reynolds et al. 2009). It has been shown that Cdt1 is

rapidly degraded at the end of G1, which is essential in preventing genome reduplication (Pozo and Cook 2016; Xouri et al. 2007). We speculate this low T_m in vitro could help promote faster unfolding and proteasome degradation, which could potentially have implications for Cdt1's rapid degradation during different cell cycle stages (Bashore et al. 2015; Varma et al. 2012).

TABLE 2 | Rg, χ^2, and WHD center-of-mass distances of representative model structures.

Model	Rg (Å)	χ^2	Center-of-mass distance between WH domains (Å)
1	31	6.3	24
2	40	5.5	59
3	72	14.8	153
4	41	1.7	39

Spectroscopy experiments confirmed that Cdt1 has a high disorder content. Other microtubule-binding proteins like Tau, Knl1 (Audett and Maresca 2020), and TPX2 (King and Petry 2020), are well-reported to contain intrinsically disordered regions as well, all consistent with scaffold functions. The intrinsic disorder can also facilitate engagement of the proteasome (Hagai et al. 2011), which in the case of Cdt1, we again speculate could aid in rapid degradation throughout the cell cycle. In a set of 124 protein–protein complexes, one group proposed increased conformational heterogeneity and increased interface "recognition"

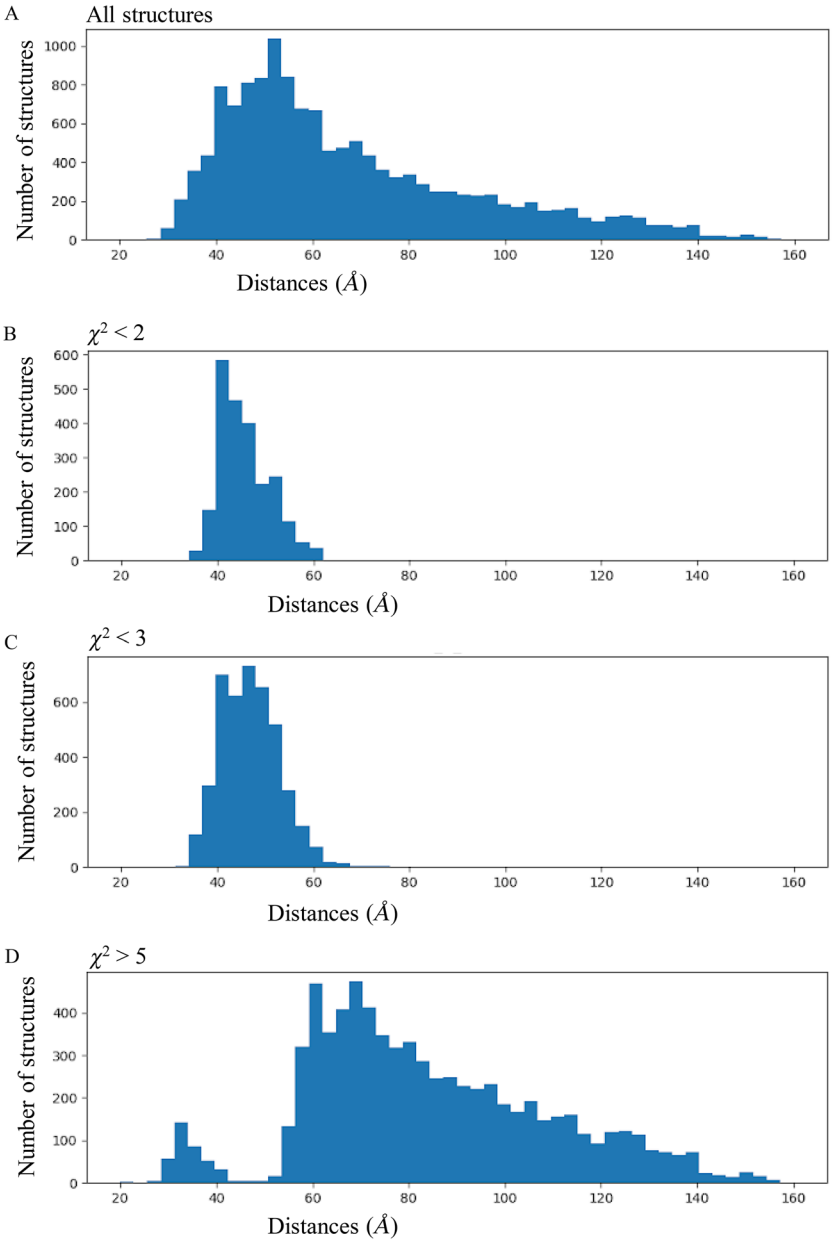

FIGURE 5 | WHM/WHC center-of-mass, inter-domain histograms. (A) Number of structures in our ensemble as a function of inter-WHD center-of-mass distances. (B) Number of structures in our ensemble as a function of inter-domain center-of-mass distances with χ^2 less than 2. (C) Number of structures in our ensemble as a function of inter-domain center-of-mass distances with χ^2 less than 3. (D) Number of structures in our ensemble as a function of inter-domain center-of-mass distances with χ^2 greater than 5.

promoted complex formation (Pallara et al. 2016), which may apply to Cdt1 as well. The relative instability of Cdt1 under different conditions could preclude more detailed studies of ionic and pH effects on the structure. While beyond the scope of this work, future studies in this area would significantly increase our understanding of inter-domain interactions or lack thereof (Barbosa et al. 2010).

Cdt1's most well-characterized mitotic binding partners, including the Ndc80 and Ska1 protein complexes, have been shown to homo-oligomerize on microtubules or in the presence of their binding partners to accomplish their mitotic functions (Alushin et al. 2010; Volkov et al. 2018). Ndc80 can homo-oligomerize independently, consistent with its load-bearing role at microtubules. Our data shows, in contrast, that Cdt1 cannot independently form higher-order oligomers in vitro without its other kinetochore-binding components. A monomeric state would likely be required at the pre-replication complex to ensure only one licensing step. Both functions imply binding partner association, not high local concentration in isolation, drives Cdt1 complex formation with Ndc80, consistent with its function as a scaffold protein. Our modeling data for Cdt1 also demonstrated poor fits to conformations which are "spread apart" or "extended." This contrasts with proteins like ataxin-3, where similar SAXS/MD analyses (Sicorello et al. 2018, 2021) showed the domains and disordered tail are all separated far apart. Because ataxin-3 functions as a deubiquitinase, these conformations are proposed to help bind and cleave across extended poly-ubiquitin chains.

We hypothesize the "folded over" conformations we determined for Cdt1 could exhibit some level of steric hindrance, making it less likely to bridge kinetochore components without some level of conformational "opening up." In SAXS/MD/MC studies of TraI, the domains and linkers adopt similar "folded over" conformations, with the folded domains close to each other and the linker extended out in solution. TraI is a scaffold protein for the DNA strand transfer machinery (Matson and Ragonese 2005). Based on their data, the authors suggested this inter-domain proximity could be responsible for the observed negative cooperation between the nickase and ssDNA binding domains, which otherwise would extend apart (Wright et al. 2012). Multidomain proteins that fold over onto themselves can sometimes have auto-inhibitory functions (van Spronsen et al. 2013; Wauer and Komander 2013). Based on our SAXS/MD/MC data, and in the context of other data on mixed-folded proteins, we hypothesize that monomeric Cdt1 could potentially exist in solution in some form of an auto-inhibitory state. Cdt1 may undergo a relatively sizeable conformational change to extend and bridge multiple kinetochore components. This work further enables future reductionist approaches to study formation of the Ska/Ndc80 and MCM complexes in addition to other mixed-folded protein systems. Finally, our center-of-mass analyses may aid in future intra-molecular FRET probe studies in vitro or in cells (Dimura et al. 2016).

Author Contributions

K.P.S. and D.V. initiated the project. K.P.S. managed the project and designed the experiments. K.P.S., A.R., and K.M.V. expressed and purified proteins. M.T. collected and analyzed NMR data. M.C. collected and analyzed TIRF-M data. M.G.P. collected and analyzed DSF data. K.M.V. collected and analyzed DLS data. S.C. collected SAXS data. A.A.G. assisted in CD and SEC-MALS data collection and analysis. K.P.S. and J.E.C. performed simulations, analysis, and interpretation. D.V., A.A.G., and J.E.C. provided additional intellectual input. K.P.S. wrote the manuscript with assistance from D.V. and input from all authors.

Acknowledgments

We thank Dr. Cara Gottardi for her support and mentorship. We thank Anita Varma for laboratory operations. We thank Dr. Sergii Pshenychnyi of the Recombinant Protein Production Core for supplying TEV protease. We thank Dr. Ronald Soriano, James Casey, and the Northwestern Keck Biophysics Facility for assistance with data collection. This work used resources from the Northwestern University Keck Biophysics Facility, supported by NCI-CCSG-P30-CA060553 and was awarded to the Robert H. Lurie Comprehensive Cancer Center. This study made use of the National Magnetic Resonance Facility at Madison; an NIH Biomedical Technology Research Resource Center supported by NIH R24GM141526. Helium recovery equipment, computers, and infrastructure for data archive were funded by the University of Wisconsin-Madison, NIH P41GM136463, R24GM141526, and by the United States National Science Foundation Mid-Scale Research Infrastructure-1 Program Grant No. 1946970. Use of the Advanced Photon Source was supported by the US Department of Energy, Office of Science, Office of Basic Energy Sciences, under Contract No. DE-AC02-06CH11357. The use of Pilatus 3 1M detector was provided by grant 1S10OD018090-01 from NIGMS. This work was supported by NIGMS grant R01GM135391 to D.V.

Conflicts of Interest

The authors declare no conflicts of interest.

Data Availability Statement

The data that support the findings of this study are available from the corresponding authors upon reasonable request.

References

Afreen, S., A. Rahi, A. G. Landeros, M. Chakraborty, R. J. McKenney, and D. Varma. 2022. "In Vitro and In Vivo Approaches to Study Kinetochore-Microtubule Attachments During Mitosis." *Methods in Molecular Biology* 2415: 123–138. https://doi.org/10.1007/978-1-0716-1904-9_9.

Agarwal, S., K. P. Smith, Y. Zhou, A. Suzuki, R. J. McKenney, and D. Varma. 2018. "Cdt1 Stabilizes Kinetochore-Microtubule Attachments via an Aurora B Kinase-Dependent Mechanism." *Journal of Cell Biology* 217, no. 10: 3446–3463. https://doi.org/10.1083/jcb.201705127.

Alushin, G. M., V. H. Ramey, S. Pasqualato, et al. 2010. "The Ndc80 Kinetochore Complex Forms Oligomeric Arrays Along Microtubules." *Nature* 467, no. 7317: 805–810. https://doi.org/10.1038/nature09423.

Audett, M. R., and T. J. Maresca. 2020. "The Whole Is Greater Than the Sum of Its Parts: At the Intersection of Order, Disorder, and Kinetochore Function." *Essays in Biochemistry* 64, no. 2: 349–358. https://doi.org/10.1042/EBC20190069.

Baek, M., F. DiMaio, I. Anishchenko, et al. 2021. "Accurate Prediction of Protein Structures and Interactions Using a Three-Track Neural Network." *Science* 373, no. 6557: 871–876. https://doi.org/10.1126/science.abj8754.

Barbosa, L. R., M. G. Ortore, F. Spinozzi, P. Mariani, S. Bernstorff, and R. Itri. 2010. "The Importance of Protein-Protein Interactions on the pH-Induced Conformational Changes of Bovine Serum Albumin: A Small-Angle X-Ray Scattering Study." *Biophysical Journal* 98, no. 1: 147–157. https://doi.org/10.1016/j.bpj.2009.09.056.

Bashore, C., C. M. Dambacher, E. A. Goodall, M. E. Matyskiela, G. C. Lander, and A. Martin. 2015. "Ubp6 Deubiquitinase Controls Conformational Dynamics and Substrate Degradation of the 26S Proteasome." *Nature Structural & Molecular Biology* 22, no. 9: 712–719. https://doi.org/10.1038/nsmb.3075.

Best, R. B., X. Zhu, J. Shim, et al. 2012. "Optimization of the Additive CHARMM All-Atom Protein Force Field Targeting Improved Sampling of the Backbone phi, psi and Side-Chain chi(1) and chi(2) Dihedral Angles." *Journal of Chemical Theory and Computation* 8, no. 9: 3257–3273. https://doi.org/10.1021/ct300400x.

Borgia, A., W. Zheng, K. Buholzer, et al. 2016. "Consistent View of Polypeptide Chain Expansion in Chemical Denaturants From Multiple Experimental Methods." *Journal of the American Chemical Society* 138, no. 36: 11714–11726. https://doi.org/10.1021/jacs.6b05917.

Chan-Yao-Chong, M., D. Durand, and T. Ha-Duong. 2019. "Molecular Dynamics Simulations Combined With Nuclear Magnetic Resonance and/or Small-Angle X-Ray Scattering Data for Characterizing Intrinsically Disordered Protein Conformational Ensembles." *Journal of Chemical Information and Modeling* 59, no. 5: 1743–1758. https://doi.org/10.1021/acs.jcim.8b00928.

Chemes, L. B., L. G. Alonso, M. G. Noval, and G. de Prat-Gay. 2012. "Circular Dichroism Techniques for the Analysis of Intrinsically Disordered Proteins and Domains." *Methods in Molecular Biology* 895: 387–404. https://doi.org/10.1007/978-1-61779-927-3_22.

Curtis, J. E. R. S., N. Hirsh, and K. Susan. 2012. "SASSIE: A Program to Study Intrinsically Disordered Biological." *Computer Physics Communications* 183, no. 2: 382–389.

Datta, S. A., J. E. Curtis, W. Ratcliff, et al. 2007. "Conformation of the HIV-1 Gag Protein in Solution." *Journal of Molecular Biology* 365, no. 3: 812–824. https://doi.org/10.1016/j.jmb.2006.10.073.

Datta, S. A., F. Heinrich, S. Raghunandan, et al. 2011. "HIV-1 Gag Extension: Conformational Changes Require Simultaneous Interaction With Membrane and Nucleic Acid." *Journal of Molecular Biology* 406, no. 2: 205–214. https://doi.org/10.1016/j.jmb.2010.11.051.

de Chiara, C., R. P. Menon, F. Dal Piaz, L. Calder, and A. Pastore. 2005. "Polyglutamine Is Not all: The Functional Role of the AXH Domain in the Ataxin-1 Protein." *Journal of Molecular Biology* 354, no. 4: 883–893. https://doi.org/10.1016/j.jmb.2005.09.083.

De Marco, V., P. J. Gillespie, A. Li, et al. 2009. "Quaternary Structure of the Human Cdt1-Geminin Complex Regulates DNA Replication Licensing." *Proceedings of the National Academy of Sciences of the United States of America* 106, no. 47: 19807–19812. https://doi.org/10.1073/pnas.0905281106.

Deiana, A., S. Forcelloni, A. Porrello, and A. Giansanti. 2019. "Intrinsically Disordered Proteins and Structured Proteins With Intrinsically Disordered Regions Have Different Functional Roles in the Cell." *PLoS One* 14, no. 8: e0217889. https://doi.org/10.1371/journal.pone.0217889.

Delaglio, F., S. Grzesiek, G. W. Vuister, G. Zhu, J. Pfeifer, and A. Bax. 1995. "NMRPipe: A Multidimensional Spectral Processing System Based on UNIX Pipes." *Journal of Biomolecular NMR* 6, no. 3: 277–293. https://www.ncbi.nlm.nih.gov/pubmed/8520220.

Dimura, M., T. O. Peulen, C. A. Hanke, A. Prakash, H. Gohlke, and C. A. Seidel. 2016. "Quantitative FRET Studies and Integrative Modeling Unravel the Structure and Dynamics of Biomolecular Systems." *Current Opinion in Structural Biology* 40: 163–185. https://doi.org/10.1016/j.sbi.2016.11.012.

Dubreuil, B., O. Matalon, and E. D. Levy. 2019. "Protein Abundance Biases the Amino Acid Composition of Disordered Regions to Minimize Non-functional Interactions." *Journal of Molecular Biology* 431, no. 24: 4978–4992. https://doi.org/10.1016/j.jmb.2019.08.008.

Dunker, A. K., M. S. Cortese, P. Romero, L. M. Iakoucheva, and V. N. Uversky. 2005. "Flexible Nets. The Roles of Intrinsic Disorder in Protein Interaction Networks." *FEBS Journal* 272, no. 20: 5129–5148. https://doi.org/10.1111/j.1742-4658.2005.04948.x.

Foit, L., G. J. Morgan, M. J. Kern, et al. 2009. "Optimizing Protein Stability In Vivo." *Molecular Cell* 36, no. 5: 861–871. https://doi.org/10.1016/j.molcel.2009.11.022.

Franke, D., M. V. Petoukhov, P. V. Konarev, et al. 2017. "ATSAS 2.8: A Comprehensive Data Analysis Suite for Small-Angle Scattering From Macromolecular Solutions." *Journal of Applied Crystallography* 50, no. 4: 1212–1225. https://doi.org/10.1107/S1600576717007786.

Frigola, J., J. He, K. Kinkelin, et al. 2017. "Cdt1 Stabilizes an Open MCM Ring for Helicase Loading." *Nature Communications* 8: 15720. https://doi.org/10.1038/ncomms15720.

Fuxreiter, M. 2020. "Classifying the Binding Modes of Disordered Proteins." *International Journal of Molecular Sciences* 21, no. 22: 1–9. https://doi.org/10.3390/ijms21228615.

Gasteiger, E., A. Gattiker, S. Duvaud, M. R. Wilkins, R. D. Appel, and A. Bairoch. 2005. *Protein Identification and Analysis Tools on the ExPASy Server*. Totowa, NJ: Humana Press.

Ghaemmaghami, S., and T. G. Oas. 2001. "Quantitative Protein Stability Measurement In Vivo." *Nature Structural Biology* 8, no. 10: 879–882. https://doi.org/10.1038/nsb1001-879.

Graewert, M. A., S. Da Vela, T. W. Gräwert, et al. 2020. "Adding Size Exclusion Chromatography (SEC) and Light Scattering (LS) Devices to Obtain High-Quality Small Angle X-Ray Scattering (SAXS) Data." *Crystals* 10, no. 975: 1–18.

Greenfield, N. J. 2006. "Using Circular Dichroism Spectra to Estimate Protein Secondary Structure." *Nature Protocols* 1, no. 6: 2876–2890. https://doi.org/10.1038/nprot.2006.202.

Hagai, T., A. Azia, A. Toth-Petroczy, and Y. Levy. 2011. "Intrinsic Disorder in Ubiquitination Substrates." *Journal of Molecular Biology* 412, no. 3: 319–324. https://doi.org/10.1016/j.jmb.2011.07.024.

Hopkins, J. B., R. E. Gillilan, and S. Skou. 2017. "BioXTAS RAW: Improvements to a Free Open-Source Program for Small-Angle X-Ray Scattering Data Reduction and Analysis." *Journal of Applied Crystallography* 50, no. 5: 1545–1553. https://doi.org/10.1107/S1600576717011438.

Humphrey, W., A. Dalke, and K. Schulten. 1996. "VMD: Visual Molecular Dynamics." *Journal of Molecular Graphics* 14, no. 1: 33–38. https://doi.org/10.1016/0263-7855(96)00018-5.

Ianeselli, L., F. Zhang, M. W. Skoda, et al. 2010. "Protein-Protein Interactions in Ovalbumin Solutions Studied by Small-Angle Scattering: Effect of Ionic Strength and the Chemical Nature of Cations." *Journal of Physical Chemistry. B* 114, no. 11: 3776–3783. https://doi.org/10.1021/jp9112156.

Ito, K., and N. Matsudomi. 2005. "Structural Characteristics of Hen Egg Ovalbumin Expressed in Yeast Pichia Pastoris." *Bioscience, Biotechnology, and Biochemistry* 69, no. 4: 755–761. https://doi.org/10.1271/bbb.69.755.

Jee, J., T. Mizuno, K. Kamada, et al. 2010. "Structure and Mutagenesis Studies of the C-Terminal Region of Licensing Factor Cdt1 Enable the Identification of Key Residues for Binding to Replicative Helicase mcm Proteins." *Journal of Biological Chemistry* 285, no. 21: 15931–15940. https://doi.org/10.1074/jbc.M109.075333.

Jumper, J., R. Evans, A. Pritzel, et al. 2021. "Highly Accurate Protein Structure Prediction With AlphaFold." *Nature* 596, no. 7873: 583–589. https://doi.org/10.1038/s41586-021-03819-2.

Khayrutdinov, B. I., W. J. Bae, Y. M. Yun, et al. 2009. "Structure of the Cdt1 C-Terminal Domain: Conservation of the Winged Helix Fold in Replication Licensing Factors." *Protein Science* 18, no. 11: 2252–2264. https://doi.org/10.1002/pro.236.

Kikhney, A. G., and D. I. Svergun. 2015. "A Practical Guide to Small Angle X-Ray Scattering (SAXS) of Flexible and Intrinsically Disordered

Proteins." *FEBS Letters* 589, no. 19 pt. A: 2570–2577. https://doi.org/10.1016/j.febslet.2015.08.027.

King, M. R., and S. Petry. 2020. "Phase Separation of TPX2 Enhances and Spatially Coordinates Microtubule Nucleation." *Nature Communications* 11, no. 1: 270. https://doi.org/10.1038/s41467-019-14087-0.

Konarev, P. V., V. V. Volkov, A. V. Sokolova, M. H. J. Koch, and D. I. Svergun. 2003. "PRIMUS: A Windows PC-Based System for Small-Angle Scattering Data Analysis." *Journal of Applied Crystallography* 36: 1277–1282.

Krueger, S., J. H. Shin, J. E. Curtis, K. A. Rubinson, and Z. Kelman. 2014. "The Solution Structure of Full-Length Dodecameric MCM by SANS and Molecular Modeling." *Proteins* 82, no. 10: 2364–2374. https://doi.org/10.1002/prot.24598.

Krueger, S., J. H. Shin, S. Raghunandan, J. E. Curtis, and Z. Kelman. 2011. "Atomistic Ensemble Modeling and Small-Angle Neutron Scattering of Intrinsically Disordered Protein Complexes: Applied to Minichromosome Maintenance Protein." *Biophysical Journal* 101, no. 12: 2999–3007. https://doi.org/10.1016/j.bpj.2011.11.006.

Lee, C., B. Hong, J. M. Choi, et al. 2004. "Structural Basis for Inhibition of the Replication Licensing Factor Cdt1 by Geminin." *Nature* 430, no. 7002: 913–917. https://doi.org/10.1038/nature02813.

Lee, S. H., E. J. Cha, J. E. Lim, et al. 2012. "Structural Characterization of an Intrinsically Unfolded Mini-HBX Protein From Hepatitis B Virus." *Molecules and Cells* 34, no. 2: 165–169. https://doi.org/10.1007/s10059-012-0060-z.

Lee, W., M. Tonelli, and J. L. Markley. 2015. "NMRFAM-SPARKY: Enhanced Software for Biomolecular NMR Spectroscopy." *Bioinformatics* 31, no. 8: 1325–1327. https://doi.org/10.1093/bioinformatics/btu830.

Malaby, A. W., S. Chakravarthy, T. C. Irving, S. V. Kathuria, O. Bilsel, and D. G. Lambright. 2015. "Methods for Analysis of Size-Exclusion Chromatography-Small-Angle X-Ray Scattering and Reconstruction of Protein Scattering." *Journal of Applied Crystallography* 48, no. 4: 1102–1113. https://doi.org/10.1107/S1600576715010420.

Mathew, E., A. Mirza, and N. Menhart. 2004. "Liquid-Chromatography-Coupled SAXS for Accurate Sizing of Aggregating Proteins." *Journal of Synchrotron Radiation* 11, no. 4: 314–318. https://doi.org/10.1107/S0909049504014086.

Matson, S. W., and H. Ragonese. 2005. "The F-Plasmid TraI Protein Contains Three Functional Domains Required for Conjugative DNA Strand Transfer." *Journal of Bacteriology* 187, no. 2: 697–706. https://doi.org/10.1128/JB.187.2.697-706.2005.

Morgan, A. A., and E. Rubenstein. 2013. "Proline: The Distribution, Frequency, Positioning, and Common Functional Roles of Proline and Polyproline Sequences in the Human Proteome." *PLoS One* 8, no. 1: e53785. https://doi.org/10.1371/journal.pone.0053785.

Neira, J. L., J. Bintz, M. Arruebo, et al. 2017. "Identification of a Drug Targeting an Intrinsically Disordered Protein Involved in Pancreatic Adenocarcinoma." *Scientific Reports* 7: 39732. https://doi.org/10.1038/srep39732.

Omer Javed, A., Y. Li, J. Muffat, et al. 2018. "Microcephaly Modeling of Kinetochore Mutation Reveals a Brain-Specific Phenotype." *Cell Reports* 25, no. 2: 368–382.e5. https://doi.org/10.1016/j.celrep.2018.09.032.

Pallara, C., M. Rueda, R. Abagyan, and J. Fernandez-Recio. 2016. "Conformational Heterogeneity of Unbound Proteins Enhances Recognition in Protein-Protein Encounters." *Journal of Chemical Theory and Computation* 12, no. 7: 3236–3249. https://doi.org/10.1021/acs.jctc.6b00204.

Perkins, S. J., D. W. Wright, H. Zhang, et al. 2016. "Atomistic Modelling of Scattering Data in the Collaborative Computational Project for Small Angle Scattering (CCP-SAS)." *Journal of Applied Crystallography* 49, no. 6: 1861–1875. https://doi.org/10.1107/S160057671601517X.

Petropoulou, C., P. Kotantaki, D. Karamitros, and S. Taraviras. 2008. "Cdt1 and Geminin in Cancer: Markers or Triggers of Malignant Transformation?" *Frontiers in Bioscience* 13: 4485–4494. https://doi.org/10.2741/3018.

Phillips, J. C., R. Braun, W. Wang, et al. 2005. "Scalable Molecular Dynamics With NAMD." *Journal of Computational Chemistry* 26, no. 16: 1781–1802. https://doi.org/10.1002/jcc.20289.

Pozo, P. N., and J. G. Cook. 2016. "Regulation and Function of Cdt1; A Key Factor in Cell Proliferation and Genome Stability." *Genes (Basel)* 8, no. 1: 1–23. https://doi.org/10.3390/genes8010002.

Provencher, S. W., and J. Glockner. 1981. "Estimation of Globular Protein Secondary Structure From Circular Dichroism." *Biochemistry* 20, no. 1: 33–37. https://www.ncbi.nlm.nih.gov/pubmed/7470476.

Rahi, A., M. Chakraborty, S. Agarwal, et al. 2023. "The Ndc80-Cdt1-Ska1 Complex Is a Central Processive Kinetochore-Microtubule Coupling Unit." *Journal of Cell Biology* 222, no. 8: 1–24. https://doi.org/10.1083/jcb.202208018.

Rahi, A., M. Chakraborty, K. Vosberg, and D. Varma. 2020. "Kinetochore-Microtubule Coupling Mechanisms Mediated by the Ska1 Complex and Cdt1." *Essays in Biochemistry* 64, no. 2: 337–347. https://doi.org/10.1042/EBC20190075.

Ren, J., L. Wen, X. Gao, C. Jin, Y. Xue, and X. Yao. 2009. "DOG 1.0: Illustrator of Protein Domain Structures." *Cell Research* 19, no. 2: 271–273. https://doi.org/10.1038/cr.2009.6.

Saad Tayyab, S. Q., and M. Islam. 1991. "Size Exclusion Chromatography and Size Exclusion HPLC of Proteins." *Biochemical Education* 19, no. 3: 149–152.

Santofimia-Castano, P., B. Rizzuti, Y. Xia, et al. 2019. "Designing and Repurposing Drugs to Target Intrinsically Disordered Proteins for Cancer Treatment: Using NUPR1 as a Paradigm." *Molecular & Cellular Oncology* 6, no. 5: e1612678. https://doi.org/10.1080/23723556.2019.1612678.

Schrödinger LLC. 2020. "The PyMOL Molecular Graphics System, Version 2.0."

Shiba, K., T. Niidome, E. Katoh, et al. 2010. "Polydispersity as a Parameter for Indicating the Thermal Stability of Proteins by Dynamic Light Scattering." *Analytical Sciences* 26, no. 6: 659–663. https://doi.org/10.2116/analsci.26.659.

Sicorello, A., G. Kelly, A. Oregioni, J. Novacek, V. Sklenar, and A. Pastore. 2018. "The Structural Properties in Solution of the Intrinsically Mixed Folded Protein Ataxin-3." *Biophysical Journal* 115, no. 1: 59–71. https://doi.org/10.1016/j.bpj.2018.05.029.

Sicorello, A., B. Rozycki, P. V. Konarev, D. I. Svergun, and A. Pastore. 2021. "Capturing the Conformational Ensemble of the Mixed Folded Polyglutamine Protein Ataxin-3." *Structure* 29, no. 1: 70–81.e5. https://doi.org/10.1016/j.str.2020.09.010.

Simossis, V. A., and J. Heringa. 2005. "PRALINE: A Multiple Sequence Alignment Toolbox That Integrates Homology-Extended and Secondary Structure Information." *Nucleic Acids Research* 33: W289–W294. https://doi.org/10.1093/nar/gki390.

Smilgies, D. M., and E. Folta-Stogniew. 2015. "Molecular Weight-Gyration Radius Relation of Globular Proteins: A Comparison of Light Scattering, Small-Angle X-Ray Scattering and Structure-Based Data." *Journal of Applied Crystallography* 48, no. 5: 1604–1606. https://doi.org/10.1107/S1600576715015551.

Soares, D. C., B. C. Carlyle, N. J. Bradshaw, and D. J. Porteous. 2011. "DISC1: Structure, Function, and Therapeutic Potential for Major Mental Illness." *ACS Chemical Neuroscience* 2, no. 11: 609–632. https://doi.org/10.1021/cn200062k.

Some, D., H. Amartely, A. Tsadok, and M. Lebendiker. 2019. "Characterization of Proteins by Size-Exclusion Chromatography Coupled to Multi-Angle Light Scattering (SEC-MALS)." *Journal of Visualized Experiments* 148: 1–9. https://doi.org/10.3791/59615.

Stein, P. E., A. G. Leslie, J. T. Finch, and R. W. Carrell. 1991. "Crystal Structure of Uncleaved Ovalbumin at 1.95 A Resolution." *Journal of Molecular Biology* 221, no. 3: 941–959. https://doi.org/10.1016/0022-2836(91)80185-w.

Stelzl, L. S., L. M. Pietrek, A. Holla, et al. 2022. "Global Structure of the Intrinsically Disordered Protein Tau Emerges From Its Local Structure." *JACS Au* 2, no. 3: 673–686. https://doi.org/10.1021/jacsau.1c00536.

Sun, J., C. Evrin, S. A. Samel, et al. 2013. "Cryo-EM Structure of a Helicase Loading Intermediate Containing ORC-Cdc6-Cdt1-MCM2-7 Bound to DNA." *Nature Structural & Molecular Biology* 20, no. 8: 944–951. https://doi.org/10.1038/nsmb.2629.

Ulery-Reynolds, P. G., M. A. Castillo, V. Vialou, S. J. Russo, and E. J. Nestler. 2009. "Phosphorylation of DeltaFosB Mediates Its Stability In Vivo." *Neuroscience* 158, no. 2: 369–372. https://doi.org/10.1016/j.neuroscience.2008.10.059.

van Spronsen, M., M. Mikhaylova, J. Lipka, et al. 2013. "TRAK/Milton Motor-Adaptor Proteins Steer Mitochondrial Trafficking to Axons and Dendrites." *Neuron* 77, no. 3: 485–502. https://doi.org/10.1016/j.neuron.2012.11.027.

Varma, D., S. Chandrasekaran, L. J. Sundin, et al. 2012. "Recruitment of the Human Cdt1 Replication Licensing Protein by the Loop Domain of Hec1 Is Required for Stable Kinetochore-Microtubule Attachment." *Nature Cell Biology* 14, no. 6: 593–603. https://doi.org/10.1038/ncb2489.

Volkov, V. A., P. J. Huis In't Veld, M. Dogterom, and A. Musacchio. 2018. "Multivalency of NDC80 in the Outer Kinetochore Is Essential to Track Shortening Microtubules and Generate Forces." *eLife* 7: 1–22. https://doi.org/10.7554/eLife.36764.

Watanabe, Y., and Y. Inoko. 2009. "Size-Exclusion Chromatography Combined With Small-Angle X-Ray Scattering Optics." *Journal of Chromatography. A* 1216, no. 44: 7461–7465. https://doi.org/10.1016/j.chroma.2009.02.053.

Wauer, T., and D. Komander. 2013. "Structure of the Human Parkin Ligase Domain in an Autoinhibited State." *EMBO Journal* 32, no. 15: 2099–2112. https://doi.org/10.1038/emboj.2013.125.

Wiesner, R., C. Scheller, F. Krebs, H. Watzig, and I. Oltmann-Norden. 2021. "A Comparative Study of CE-SDS, SDS-PAGE, and Simple Western: Influences of Sample Preparation on Molecular Weight Determination of Proteins." *Electrophoresis* 42, no. 3: 206–218. https://doi.org/10.1002/elps.202000199.

Wright, N. T., M. Raththagala, C. W. Hemmis, et al. 2012. "Solution Structure and Small Angle Scattering Analysis of TraI (381-569)." *Proteins* 80, no. 9: 2250–2261. https://doi.org/10.1002/prot.24114.

Wright, P. E., and H. J. Dyson. 2015. "Intrinsically Disordered Proteins in Cellular Signalling and Regulation." *Nature Reviews. Molecular Cell Biology* 16, no. 1: 18–29. https://doi.org/10.1038/nrm3920.

Xouri, G., M. Dimaki, P. I. Bastiaens, and Z. Lygerou. 2007. "Cdt1 Interactions in the Licensing Process: A Model for Dynamic Spatiotemporal Control of Licensing." *Cell Cycle* 6, no. 13: 1549–1552. https://doi.org/10.4161/cc.6.13.4455.

Yao, J., H. J. Dyson, and P. E. Wright. 1997. "Chemical Shift Dispersion and Secondary Structure Prediction in Unfolded and Partly Folded Proteins." *FEBS Letters* 419, no. 2–3: 285–289. https://doi.org/10.1016/s0014-5793(97)01474-9.

Yuan, Z., A. Riera, L. Bai, et al. 2017. "Structural Basis of Mcm2-7 Replicative Helicase Loading by ORC-Cdc6 and Cdt1." *Nature Structural & Molecular Biology* 24, no. 3: 316–324. https://doi.org/10.1038/nsmb.3372.

Yuan, Z., S. Schneider, T. Dodd, et al. 2020. "Structural Mechanism of Helicase Loading Onto Replication Origin DNA by ORC-Cdc6." *Proceedings of the National Academy of Sciences of the United States of America* 117, no. 30: 17747–17756. https://doi.org/10.1073/pnas.2006231117.

Zhai, Y., E. Cheng, H. Wu, et al. 2017. "Open-Ringed Structure of the Cdt1-Mcm2-7 Complex as a Precursor of the MCM Double Hexamer." *Nature Structural & Molecular Biology* 24, no. 3: 300–308. https://doi.org/10.1038/nsmb.3374.

Zheng, W., and R. B. Best. 2018. "An Extended Guinier Analysis for Intrinsically Disordered Proteins." *Journal of Molecular Biology* 430, no. 16: 2540–2553. https://doi.org/10.1016/j.jmb.2018.03.007.

Supporting Information

Additional supporting information can be found online in the Supporting Information section.